

TESTING AND MODELLING STRATEGY FOR APPLICATION-ORIENTED SERVICE STRENGTH ANALYSIS OF COMPOSITE MATERIALS IN HYBRID ADHESIVE JOINTS

K. Tittmann¹, J. Wacker², I. Koch¹, M. Gude¹ and T. Melz²

¹ Institute of Lightweight Engineering and Polymer Technology, Technische Universität Dresden
Holbeinstraße 3, 01307 Dresden, Germany, Email: karsten.tittmann@tu-dresden.de, Web Page:
<https://tu-dresden.de/ing/maschinenwesen/ilk>

²System Reliability, Adaptive Structures and Machine Acoustics, Technische Universität Darmstadt
Magdalenenstraße 4, 64289 Darmstadt, Email: wacker@sam.tu-darmstadt.de, Web Page:
<http://www.sam.tu-darmstadt.de>

Keywords: fibre reinforced plastics, adhesive joints, service strength.

Abstract

In order to exploit the full lightweight potential of hybrid adhesive joints, application orientated dimensioning and assessment methods need be developed further. This refers in particular to fatigue loading of hybrid joints under multi-axial stress states which generate significant out-of-plane stresses in the fibre reinforced component. The work presented here focuses on the CFRP material in so called semi-structural hybrid adhesive joints, in which a thick layer of polyurethane adhesive is used to bond the material to the joining partner aluminium. A testing strategy is proposed including in-plane and out-of-plane characterisation of the CFRP under static and cyclic loading as well as specific methods for service strength prediction. Finally, an outlook is given on the superordinate meta modelling strategy which incorporates a sophisticated submodel of the entire hybrid joint to provide precalculated results for efficient service strength analysis on full structure scale.

1. Introduction

In the field of mobility, multi-material design of vehicle structures combining different materials offers new lightweight potential and enables a reduction in fuel consumption and emission. Apart from hybrid metal combinations such as steel-aluminium, carbon fibre reinforced plastics (CFRP) are increasingly being combined with metal structures [1]. Therefore, joining technologies play a key role. In this context, adhesive joints, using cold-curing elastic adhesives, show good performance with respect to structural integrity and manufacturing [2]. New polyurethane adhesives with relatively high strength and stiffness are increasingly used in so called semi-structural adhesive joints, which can be applied with up to 5 mm of adhesive layer thickness [3].

Compared to homogeneous isotropic materials, adhesive joints with CFRP components can show much more complex failure mechanisms due to their inhomogeneity and anisotropy [4]. Apart from adhesive and cohesive failure, multiple failure modes such as matrix failure near the interface or delamination can occur, as illustrated in Fig. 1.

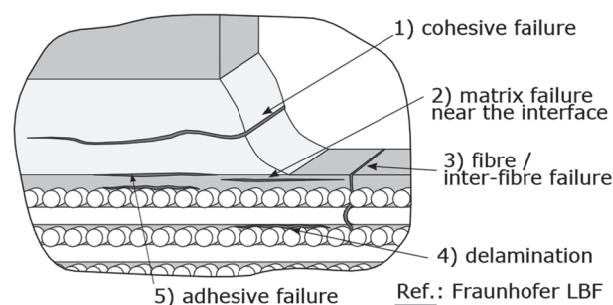


Figure 1. Illustration of possible failure mechanisms of hybrid adhesive joints with FRP components.

Extensive efforts have been made to develop different models for the lifetime prediction under constant amplitude loading [5-7]. For the prediction of the damage behaviour during fatigue loading with variable amplitudes and multiaxial stress states comprising significant out-of-plane stresses typically for adhesive joints these models need to be adapted for a computationally efficient service strength analysis.

2. Material

The investigations are performed with the unidirectional prepreg material HexPly® M79/34%/UD300/CHS [8] provided by Hexcel Corporation, which is designed for applications with large wall thickness. Sheet material with different layups for in-plane characterisation (sheet material) and unidirectional prismatic blocks for out-of-plane characterisation (block material) are manufactured.

Sheet Material

The CFRP material for in-plane characterisation is manufactured by an autoclave process in two different configurations, $[90]_7$ and $[(45/-45)_2]_8$. The laminated sheets with dimensions $500 \times 500 \text{ mm}^2$ are cured at $80 \text{ }^\circ\text{C}$ for 4 hours in the autoclave and additionally post-cured at $80 \text{ }^\circ\text{C}$ for 4 hours in a convection oven. During the autoclave process the vacuum is held the entire process and the pressure is set to 5 bar for the curing cycle. For the heating (1 K/min) and cooling process (2 K/min) corresponding pressure ramps from/to ambient pressure are used. The total autoclave process duration is 5.5 h. Preliminary manufacturing tests showed an improved surface quality by using a fine peel compared to laminates manufactured without. Better ventilation prevents surface defects such as air inclusions and creates a homogeneous surface. Further, this approach guarantees a grease-free activated surface for the subsequent adhesive joining of test coupons by removing the peel ply shortly before bonding. For the unidirectional layup $[90]_7$ a mean thickness of 2.00 mm and for the bidirectional layup $[(45/-45)_2]_8$ of 2.31 mm are measured including peel plies.

Block Material

For manufacturing the block material for out-of-plane characterisation it is necessary to adapt the autoclave process to a hot press process. Due to the large material volume of the CFRP cubical block material, the exothermic crosslinking reaction of the resin system can result in elevated temperatures in the centre of the material. As a result, this can lead to material degradation and residual stresses. Accounting this problem the curing temperature and time are slightly adjusted (480 min at $70 \text{ }^\circ\text{C}$), guaranteeing consolidation at the material boundaries and yet preventing relevant elevated temperatures in the centre. It is shown by measurements, that the centre temperature is only elevated by approx. 8 K compared to the block boundary while the maximum centre temperature is $85.2 \text{ }^\circ\text{C}$. Thus, a critical temperature increase has been avoided.

The unidirectional reinforced block material with the dimensions $100 \times 100 \times 92 \text{ mm}^3$ is manufactured according to the individual steps (Fig. 2):

1. Cutting of 352 layers on CNC cutting machine
2. Stacking of 16-layer stacks (total 22)
3. Intermediate compacting in a die by applying pressure and vacuum in laboratory press
4. Loading the cubic tool with the 16-layer stacks
5. Intermediate compaction after 5 packages each by applying pressure and vacuum
6. Curing in tool under vacuum and pressure
7. Demoulding of the block material
8. Post-curing in the convection oven

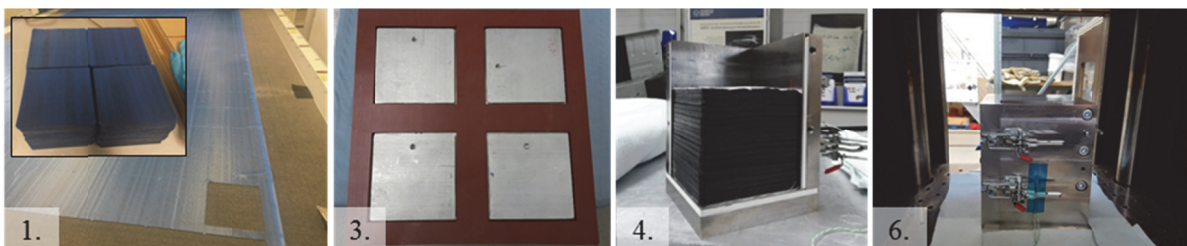


Figure 2. Manufacturing steps of the unidirectional block material.

Manufacturing is accompanied with quality analyses, which include computer tomography, three-dimensional optical metrology and reflected light microscopy for analysing pore content, fibre volume fraction, fibre orientation, surface quality, total thickness and layer thickness.

The microscopy results confirm that the set process parameters guarantee a pore-free laminate with reproducible constant thickness. The analysis of the fibre volume fraction based on the grey scale analysis of the digital image of the polished cut in MATLAB[®] shows that a fibre volume content of 58.8% vol. is achieved. Computed tomography (CT) investigations are conducted to analyse the pore content and fibre orientation of the manufactured block material. Parallel fibre orientations are observed inside the cube, whereas significant fibre displacements occur at the boundaries due to resin flow during consolidation.

3. Testing strategy and experimental results

Quasi-static tests in-plane

In order to determine the in-plane material properties such as YOUNG's modulus and ultimate strength of the unidirectional ply, quasi-static tests are carried out. Specific specimens for the individual load situations are manufactured. The loads are applied with a constant displacement of 1 mm/min. For strain measurement digital image correlation is used. The test conditions to determine tensile and compressive properties are based on [9] and [10], respectively. For the determination of shear properties the test method suggested in [11] is modified using unidirectional $[90]_7$ and cross ply $[0/90]_{8s}$ V-notched specimens (see Fig. 3). The shear moduli G_{12} determined for the different types of specimens are identical. For the $[90]_7$ specimens, the average failure stress is 49 MPa (Fig. 3 left). In the case of $[0/90]_{8s}$ specimens (Fig. 3 right), the stress-strain curves show a significant drop in stiffness starting at 49 MPa, which is defined as ultimate shear strength R_{12} , reaching ultimate fibre failure above 80 MPa.

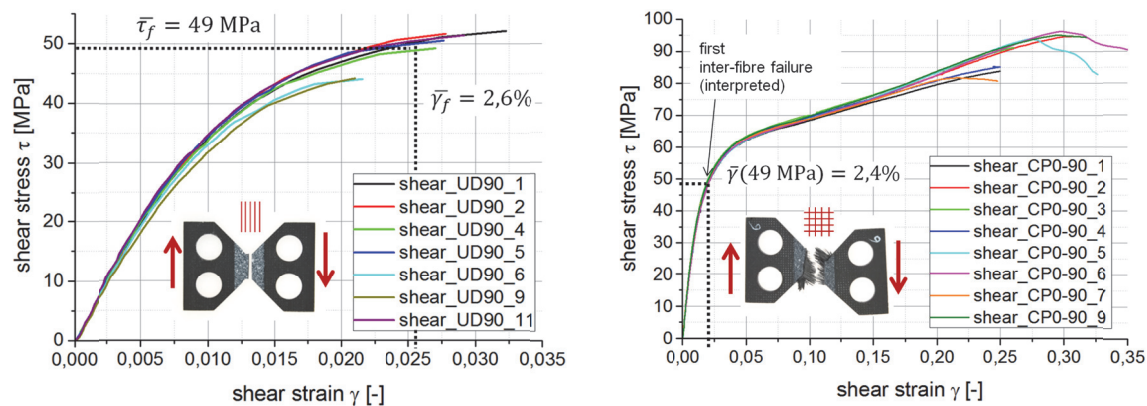


Figure 3. Results of shear tests on unidirectional $[90]_7$ (left) and cross ply $[0/90]_{8s}$ (right) specimens.

The coefficients of linear thermal expansion α_1 and α_2 were determined according to [12]. In Table 3 all quasi-static test results including the in-plane characterisation are summarised.

Fatigue tests in-plane

An overall characterisation of the fatigue life of the CFRP material is not the main focus of the present project. However, a reduced examination of the fatigue life of a single ply, in particular under transverse and shear loads, is important for the numerical model of the adhesive joint. Therefore, uniaxial fatigue tests on transverse unidirectional specimens $[90]_7$ and cross ply specimens $[+45/-45]_{8s}$ are carried out. Following the suggestion of [13], the characterisation of the single ply in the transverse direction is performed under constant strain amplitudes to take into account the predominantly strain-controlled loading situation of a transverse ply embedded in a multi-directional laminate. The strain measurement is realised using a clip gauge. First inter-fibre failure is defined as the failure criterion.

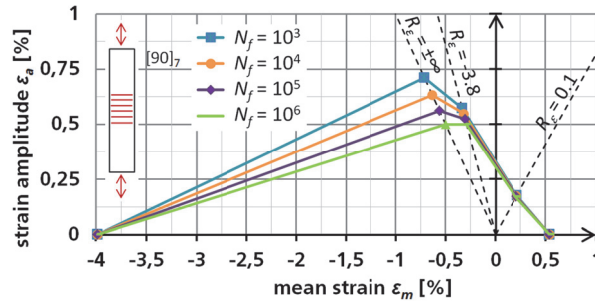


Figure 4. Haigh diagram for transverse unidirectional fibre direction.

For fatigue life characterisation of the transverse direction, strain-life curves are determined for three different strain ratios R_ε using the $[90]_7$ specimens. R_ε is defined as ratio of the minimum and maximum strain $\varepsilon_{\min}/\varepsilon_{\max}$. In addition to tensile fatigue loading with $R_\varepsilon = 0.1$ and compressive fatigue loading with $R_\varepsilon = \pm\infty$, a strain-life-curve is also generated with cyclic strain ratio $R_\varepsilon = -3.8$, which is calculated as the critical ratio of the ultimate compressive and tensile strengths R_{22}^-/R_{22}^+ .

The Haigh diagram for transverse loading (Fig. 4) shows the influence of the different strain ratios R_ε on fatigue life. The differences between the constant life curves are more pronounced for compressive fatigue loadings such as $R_\varepsilon = \pm\infty$ compared to tensile fatigue loadings such as $R_\varepsilon = 0.1$.

For fatigue life characterisation of intra-laminar shear strain loading, $[+45/-45]_{8s}$ specimens are used according to [14]. Fig. 5 left shows an exemplary stiffness curve of the fatigue test at $R_\varepsilon=0.1$. Complete failure of the specimen occurs after multiple inter-fibre failures and widespread delamination reducing the stiffness by approximately 40%. In order to identify first inter-fibre failure, the surface of the specimen is monitored using a camera system, taking pictures every 500 cycles at maximum strain. The specimens show reproducible damage evolution where first inter-fibre failure can be detected on the top plies of the specimens after approximately 10 to 20% reduction in stiffness. The strain-life curve using this visual detection method as the failure criterion is shown in Fig. 5 right. The results of fatigue life tests are summarised in Table 1.

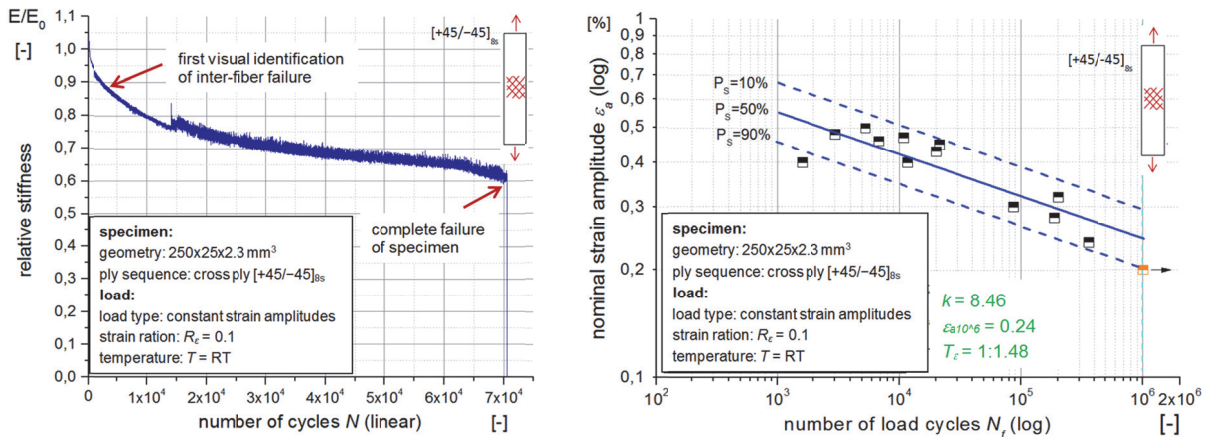


Figure 5. Characteristic stiffness degradation curve for an exemplary $[+45/-45]_{8s}$ specimen (left), Strain-life curve of with visual identification of inter-fibre-failure as failure criterion (right).


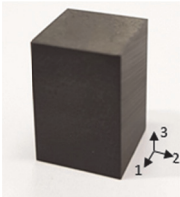
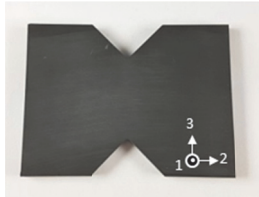
Table 1. Results of fatigue life tests on transverse unidirectional $[90]_7$ and cross ply $[+45/-45]_{8s}$ specimens under constant strain amplitudes for different strain ratios R_ε .

ply sequence of specimens	-	$[90]_7$	$[90]_7$	$[90]_7$	$[+45/-45]_{8s}$
strain ratio	R_ε	0.1	-3.8	$\pm\infty$	0.1
slope	k	193.80	49.75	19.51	8.46
strain amplitude at $N_f = 10^6$	ε_{a10^6}	0.17	0.50	0.58	0.24
span of scatter	T_ε	1:1.10	1:1.09	1:1.18	1:1.48

Out-of-plane tests

For the complete description of single layer properties for the material and failure models used in paragraph 3, determination of the material properties in thickness direction is required. This includes the elasticity parameters E_3 , G_{23} , ν_{32} and ν_{31} and the corresponding strengths R_3^+ , R_3^- , R_{23} . Digital image correlation is used for strain assessment. An overview of the tested out-of-plane specimen specifications is given in Table 2.

Table 2. Out-of-plane specimen geometries and specifications.

<i>Tension</i>	<i>Compression</i>	<i>Shear</i>
		
16 mm x 16 mm x 90 mm	10 mm x 10 mm x 25 mm	76 mm x 56 mm x 4 mm (acc. ASTM D7078 - 12)

The through-thickness tension strength of fibre composites is very sensitive to the testing method and specimen shape. Only few standardised approaches are described in literature. Therefore, a novel specimen is developed based on the geometries described in [15, 16]. For this purpose, a numerical study on alternative specimen geometries was conducted, see Fig. 6. The stress concentration factor K_t , defined as the ratio of the highest occurring stress to the nominal stress in the smallest cross section, is reduced for the novel tapered specimen with square cross-section from 1.17 to 1.06 and a homogeneous strain field is created in the analysis area (10 mm). For load application thick metal end-tabs with threads are adhesively bonded to the specimen using the adhesive Scotch-Weld™ DP490.

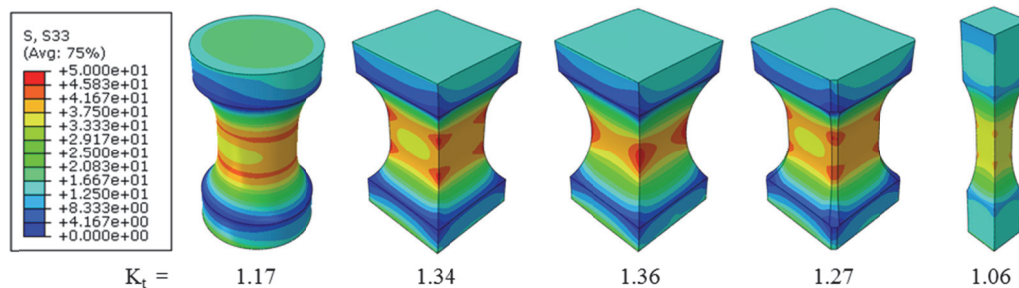


Figure 6. Study on specimen geometries, FEM results of σ_{33} and stress concentration factor.

According to ASTM D7291 the tests are performed at a constant crosshead displacement rate of 0.1 mm/min and the YOUNG'S modulus is analysed for strain points between 500 $\mu\epsilon$ and 1500 $\mu\epsilon$. The tested stress-strain curves are compared to subsequent compression tests in Fig. 7 and the results for E_3^+ , R_3^+ , ν_{31} and ν_{32} are given in Table 3.

For out-of-plane compression tests, methods developed at the Institute of Lightweight Engineering and Polymer Technology are used [17]. For load application, waisted steel compression stamps are employed to introduce a homogenous compressive stress field. Due to the small sample size, the strain assessment is performed by digital image correlation averaging over 10 x 10 mm². The testing speed is set to 0.5 mm/min and the YOUNG'S modulus is analysed in the strain range between 500 $\mu\epsilon$ and 2500 $\mu\epsilon$. The experimental results are shown in Fig. 7. The failure pattern of the damaged specimen show one dominating inter fibre crack that propagates at an angle of approximately 60°. This corresponds to the expectation from studies performed by GONZÁLEZ [18]. In his work a similar carbon fibre composite was investigated in micromechanical RVE simulations, which predicted bands of intense plastic deformation in the matrix, inclined at an angle of 52.5°.

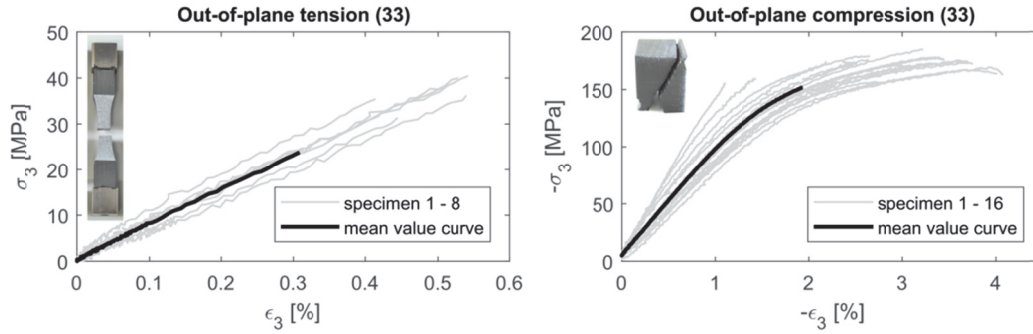


Figure 7. Experimental results of the out-of-plane tension (left) and compression (right) tests and the corresponding failure pattern.

The comparison of the tension and compression results in Fig. 7 show differences in the stress strain behaviour. Higher YOUNG'S moduli are determined for the compression tests, cf. Table 3. This can be explained by the small volume of the compression specimen and boundary effects caused by load application and friction between the compression stamps and the specimen. However, significant scatter ($s_{E_3^-} = 2.478 \text{ GPa}$) is observed for the compression YOUNG'S modulus E_3^- . Comparing $E_3^+ = 7.715 \text{ GPa}$ and $E_3^- = 9.767 \text{ GPa}$ shows that E_3^- is within the scatter band of E_3^- . Hence, E_3^+ is used for subsequent material and FEM modelling. Further, the results show good agreement in terms of stiffness and strength to the in-plane results when ideal transverse isotropy is assumed, see E_2^+/E_3^+ , R_2^+/R_3^+ and R_2^-/R_3^- in Tab. 3. However, the results indicate that the tested prepreg material is not ideally transversely isotropic. Slight deviations in stiffness and strength are caused by stacking of the prepreg plies, but also by the different test methods used for in-plane and out-of-plane characterisation. Through thickness shear properties G_{23} and R_{23} (Table 3) are tested with the V-notched rail shear method according to [19] on specimens shown in Table 2. A modified test device based on the work of Gude et al. [20] is used. The tests are performed at a crosshead speed of 1 mm/min. The failure pattern reveals that the method is appropriate for evaluating the stiffness, but that the transverse shear strength R_{23} cannot be evaluated directly. In agreement with numerical simulations, failure modes occurred in the experiments in which the cracks do not propagate from notch to notch, but inclined at an angle of about 45° from the notch towards clamping. Since this failure mode is not clearly described as an acceptable mode in the standard and the cross section for stress calculation is not defined, the 0.2% offset shear strength prescribed in [19] is used. The complete set of stiffness and strength properties of the unidirectional material is provided in Table 3.

Table 3. Summary of the elastic and strength properties of the tested prepreg UD-ply (HexPly® M79/34%/UD300/CHS with 58.8% fibre volume fraction).

Value (Units)	E_1^+ (GPa)	E_1^- (GPa)	E_2^+ (GPa)	E_2^- (GPa)	E_3^+ (GPa)	E_3^- (GPa)	G_{12} (GPa)	G_{23} (GPa)
Mean	121.6	113.5	7.566	8.294	7.715	9.767	4.051	2.488
Std. dev.	7.331	5.187	0.155	0.174	0.893	2.478	0.146	0.265
Value (Units)	R_1^+ (MPa)	R_1^- (MPa)	R_2^+ (MPa)	R_2^- (MPa)	R_3^+ (MPa)	R_3^- (MPa)	R_{12} (MPa)	R_{23}^{**} (MPa)
Mean	1452	637.9	41.17	153.7	31.752	171.304	48.51	38.912
Std. dev.	67.03	32.27	1.407	3.662	6.870	8.100	3.213	6.226
Value (Units)	ν_{12} (-)	ν_{21} (-)	ν_{13}^* (-)	ν_{31} (-)	ν_{23}^* (-)	ν_{32} (-)	α_{11} ($10^{-6}/\text{K}$)	α_{22} ($10^{-6}/\text{K}$)
Mean	0.251	0.026	0.484	0.031	0.473	0.481	0.5	38.2
Std. dev.	0.044	0.006		0.009		0.021	-	-

** 0.2% offset strength according to ASTM standard D7078

* calculated from out-of-plane tension

4. Fatigue life model for CFRP

For the service strength analysis of hybrid adhesively bonded joints a life prediction of the CFRP joining partner has to be provided. Here an energy based approach is pursued which assumes linear elastic and ideally brittle material behaviour. Based on that, the span of the normalised strain energy density ΔW^* can be rewritten in terms of the span of the squared material effort F :

$$\Delta W^*(N) = \sum \Delta(F^2). \quad (1)$$

For the experimentally determined span of the normalised strain energy density $\Delta W^*(N)$ a WÖHLER-like formulation according to the wearout-model suggested in [21] is used. The layer wise material efforts are calculated according to the fracture mode related failure conditions, which are based on the Failure Mode Concept (FMC) by CUNTZE [22]. By the quadratic summation for all failure modes a fatigue failure initiation model can be derived according to:

$$\Delta W^*(N) = \Delta((F^{\parallel\sigma})^2) + \Delta((F^{\parallel\tau})^2) + \Delta((F^{\perp\sigma})^2) + \Delta((F^{\perp\tau})^2) + \Delta((F^{\perp\perp})^2). \quad (2)$$

By solving the inverse problem the fatigue life for arbitrary combinations of amplitudes and mean stresses can be found. Realistic service loads are further on considered by applying linear accumulation according to MINER/PALMGREN:

$$D(n_k) = \sum_{i=1}^k \frac{n_i}{N_i}. \quad (3)$$

This modelling approach is further on incorporated into a superordinate meta modelling strategy. A sophisticated submodel of the bonded joint is used for precalculating the fatigue life of the whole joint including CFRP bonding partner. By application of the presented fatigue life model the probability of failure and the cycles to failure in the CFRP all failure modes is predicted for a set of predefined load combinations. A multidimensional load cycle dependent failure surface for arbitrary fatigue loadings of the bonded joint is gained and stored. On the level of the coarse full car body analysis, the service loads of the adhesive joints are calculated in a linear elastic manner according to existing standards and then evaluated against the gained load cycle dependent failure surface for efficient life prediction by means of linear damage accumulation.

5. Summary

The presented study focuses on providing a testing and modelling strategy for practice-oriented service strength analysis of CFRP in hybrid adhesive joints. For this, first an efficient and reproducible manufacturing process for in-plane and out-of-plane specimens with accompanying quality control is presented. The proposed testing strategy includes in-plane and out-of-plane tests under static and cyclic loading to generate a complete set of input parameters required for modelling fatigue life of CFRP materials in adhesive joints. The comparison of the tested properties between the transverse in-plane and the out-of-plane direction showed minor differences in stiffness and strength. The evaluated differences indicate non ideal transverse isotropic material behaviour, which needs to be considered for a safe service life prediction of composite materials. The gained experimental data is used for modelling the fatigue life until crack initiation using energy based approaches and linear damage accumulation. Finally, an outlook is given on the superordinate meta modelling strategy which incorporates the fatigue life model for CFRP and offers significant potential for an efficient service strength analysis of adhesive joints in hybrid structures. Future work will focus on application and validation of the presented modelling approach on subcomponents.

Acknowledgments

The authors gratefully acknowledge the financial support granted by numerous industrial partners and the Federal Ministry for Economic Affairs and Energy Germany in cooperation with the German Federation of Industrial Research Associations (AiF) within the project LaHyb (IGF-No. 19187 BG), as well as the collaboration with the colleagues from LWF Paderborn and IFAM Bremen.

References

- [1] N. Vila, J. Burkhardt and C. Birenbaum. Multi-material design for the optimization of the automotive production process. *15. Internationales Stuttgarter Symposium*, 419-436, 2015.
- [2] S. Grunder, S. Schmatloch and A. Lutz. Polyurethanklebstoffe zum Kleben von Kunststoffen. *Kunststoffe erfolgreich kleben – Grundlagen, Klebstofftechnologien, Best-Practice-Beispiele*. Wiesbaden: Marlene Doobe, 189-206, 2018
- [3] M. Wünsche, K. Henkel, D. Teutenberg and G. Meschut. Auslegung geklebter Kunststofffügeteile. *Kunststoffe erfolgreich kleben – Grundlagen, Klebstofftechnologien, Best-Practice-Beispiele*. Wiesbaden: Marlene Doobe, 123-140, 2018
- [4] G. Meschut, M. Wünsche, A. Matzenmiller and M. Schmerbauch. Beanspruchungs- und fertigungsgerechtes Kleben von Faserverbundwerkstoffen im Multi-Material-Design. *Verlag und Vertriebsgesellschaft mbh, FOSTA P961*, 2015
- [5] J. Degrieck and W. van Paepegem. Fatigue Damage Modelling of Fibre-reinforced Composite Materials: Review. *Applied Mechanics Reviews* 54 (4), 279–300, 2001.
- [6] I. Koch and M. Gude. Multiaxial fatigue of unidirectional ply: An experimental top-down approach. *Fatigue of Textile composites*, 105-126, 2015.
- [7] I. Koch, M. Zschoyge, K. Tittmann and M. Gude. Numerical fatigue analysis of CFRP components. *Composite Structures*, vol. 168, 392-401, 2017.
- [8] Hexcel Corporation. Product data sheet HexPly® | M79/34%/UD300/CHS. Stamford, Hexcel Corporation, 2014.
- [9] *DIN EN ISO 527-5:2010-01 – Plastics – Determination of tensile properties – Part 5: Test conditions for unidirectional fibre-reinforced plastic composites*, 2010.
- [10] *DIN EN ISO 14126:2000-12 – Fibre-reinforced plastic composites – Determination of compressive properties in the in-plane direction*, 2000.
- [11] *ASTM D5379 / D5379M-12 – Standard Test Method for Shear Properties of Composite Materials by the V-Notched Beam Method*.
- [12] *ISO 11359-2:1999-10 – Plastics – Thermomechanical analysis (TMA) – Part 2: Determination of coefficient of linear thermal expansion and glass transition temperature*.
- [13] J. Garbe and Puck A. *Erfahrungen mit Bruchkriterien an schwelend belasteten GFK-Drehfedern*. *Kunststoffe*, 83(5):406–11, 1993.
- [14] *DIN EN ISO 14129:1998-02 – Fibre-reinforced plastic composites – Determination of the in-plane shear stress/shear strain response, including the in-plane shear modulus and strength, by $\pm 45^\circ$ tension test method*.
- [15] R. Olsson. A survey of test methods for multiaxial and out-of-plane strength of composite laminates. *Composites Science and Technology*, 71:773-783, 2011.
- [16] *D7291 / D7291M-15 – Through-Thickness “Flatwise” Tensile Strength and Elastic Modulus of a Fiber-Reinforced Polymer Matrix Composite Material*, 2015.
- [17] M. Gude, R. Schirner, D. Weck, E. Dohmen and M. Andrich. Through-thickness compression testing of fabric reinforced composite materials: Adapted design of novel compression stamps. *Polymer Testing*, 56:269-276, 2016.
- [18] C. González and J. LLorca. Mechanical behavior of unidirectional fiber-reinforced polymers under transverse compression: Microscopic mechanisms and modeling. *Composites Science and Technology*, 67:2795-2806, 2007.
- [19] *ASTM D 7078 – Standard Test Method for Shear Properties of Composite Materials by V-Notched Rail Shear Method*, 2005.
- [20] M. Gude, W. Hufenbach, M. Andrich, A. Mertel and R. Schirner. Modified V-notched rail shear test fixture for shear characterisation of textile-reinforced composite materials. *Polymer Testing*, 43: 147-153, 2015.
- [21] VDI Verein Deutscher Ingenieure e.V. *Entwicklung von Bauteilen aus Faser-Kunststoff-Verbund (VDI 2014)*, Blatt 3. VDI-Richtlinie, 2006.
- [22] R. Cuntze and A. Freund. The predictive capability of failure mode concept-based strength criteria for multi-directional laminates, *Composites Science and Technology*, 64:343-377, 2004.